

Cite this: *Dalton Trans.*, 2014, **43**, 1550

# Preparation and characterization of a novel Wells–Dawson heteropolyacid-based magnetic inorganic–organic nano hybrid catalyst $H_6P_2W_{18}O_{62}$ /pyridino- $Fe_3O_4$ for the efficient synthesis of 1-amidoalkyl-2-naphthols under solvent-free conditions

Reza Tayebee,<sup>\*a</sup> Mostafa M. Amini,<sup>b</sup> Hooriyeh Rostamian<sup>a</sup> and Azam Aliakbari<sup>b</sup>

A novel magnetic inorganic–organic nano hybrid material  $H_6P_2W_{18}O_{62}$ /pyridino- $Fe_3O_4$  (HPA/TPI- $Fe_3O_4$ ) was fabricated and performed as an efficient, eco-friendly, and highly recyclable catalyst for the solvent-free, one-pot, and multi-component synthesis of various substituted 1-amidoalkyl-2-naphthols from the reaction of  $\beta$ -naphthol, an aldehyde, and benzamide with good to excellent yields (47–94%) and in a short span of time (25–60 min). The nano hybrid catalyst was prepared by the chemical anchoring of Wells–Dawson heteropolyacid  $H_6P_2W_{18}O_{62}$  onto the surface of modified  $Fe_3O_4$  nanoparticles with *N*-[3-(triethoxysilyl)propyl]isonicotinamide (TPI) linker. The magnetically recoverable catalyst was easily recycled at least eight times without any loss of catalytic activity. XRD, TEM, UV-vis, and FTIR confirmed that the heteropolyacid  $H_6P_2W_{18}O_{62}$  is well dispersed on the surface of the solid support and its structure is retained after immobilization on the pyridine modified  $Fe_3O_4$  nanoparticles. This protocol is developed as a safe and convenient alternate method for the synthesis of 1-amidoalkyl-2-naphthols utilizing an eco-friendly, and a highly reusable catalyst.

Received 15th June 2013,  
Accepted 7th October 2013

DOI: 10.1039/c3dt51594j

www.rsc.org/dalton

## 1 Introduction

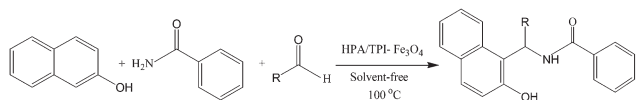
1-Amidoalkyl-2-naphthols and their derivatives bearing 1,3-amino oxygenated functional groups have attracted intense attention due to their ubiquitous role as essential building blocks for a variety of biologically important natural products, synthetic pharmaceuticals, and potent drugs, including a number of nucleoside antibiotics and HIV protease inhibitors.<sup>1,2</sup> These compounds can be converted into important ‘drug-like’ materials by amide hydrolysis and formation of 1-aminoalkyl-2-naphthols. The hypertensive and broad cardiac effects of these substrates and their potential biological activities, including antibiotic,<sup>3</sup> antitumor,<sup>4</sup> analgesic,<sup>5</sup> anti-convulsant,<sup>6</sup> antipsychotic,<sup>7</sup> antimalarial,<sup>8</sup> antianginal,<sup>9</sup> anti-hypertensive,<sup>10</sup> and antirheumatic<sup>11</sup> properties have been evaluated extensively.

Preparation of 1-amidoalkyl-2-naphthols can be carried out by condensation of aliphatic and/or aromatic aldehydes,  $\beta$ -naphthol, and acetonitrile or amides in the presence of Lewis or Brønsted acid catalysts such as montmorillonite K10 clay,<sup>12</sup> trichloroacetic acid and cobalt(II) chloride,<sup>13</sup>  $P_2O_5$ ,<sup>14</sup>  $K_5CoW_{12}O_{40}\cdot 3H_2O$ ,<sup>15</sup> sulfamic acid/ultrasound,<sup>16</sup>  $HClO_4$ - $SiO_2$ ,<sup>17</sup> cation-exchanged resins,<sup>18</sup> polymer-supported sulfonic acid (NKC-9),<sup>19</sup> silica-sulfuric acid,<sup>20</sup> Nano-S ( $S_8$ -NP),<sup>21</sup>  $Sr(OTf)_2$ ,<sup>22</sup>  $ZrOCl_2$ ,<sup>23</sup> oxalic acid,<sup>24</sup>  $Mg(ClO_4)_2$ ,<sup>25</sup> dodecylphosphonic acid (DPA),<sup>26</sup> and wet cyanuric chloride.<sup>27</sup> However, some of these catalysts suffer from the drawback from the perspective of green chemistry such as prolonged reaction times,<sup>28–33</sup> using carcinogenic solvents,<sup>28–31</sup> unsatisfactory yields,<sup>32–35</sup> toxicity and reusability of highly acidic and expensive catalysts.<sup>28,36,37</sup> Therefore, proposing clean procedures and utilizing eco-friendly and efficient catalysts which can be simply recycled at the end of the reaction have been under permanent attention.

Super paramagnetic  $Fe_3O_4$  nanoparticles, that can be magnetized in the presence of an external magnet, have attracted worldwide attention and have been studied extensively due to their biological and technological applications such as drug

<sup>a</sup>Department of Chemistry, School of Sciences, Hakim Sabzevari University, Sabzevar 96179-76487, Iran. E-mail: Rtayebee@yahoo.com; Fax: +98-571-4410300; Tel: +98-571-4410310

<sup>b</sup>Department of Chemistry, Shahid Beheshti University, G.C., Tehran 1983963113, Iran



**Scheme 1** General formulation for the preparation of different 1-amidoalkyl-2-naphthols.

delivery,<sup>38,39</sup> magnetic resonance imaging (MRI),<sup>40</sup> bioseparation,<sup>41,42</sup> biomolecular sensors<sup>43,44</sup> and magneto-thermal therapy.<sup>45,46</sup> Recent reports show that magnetic nanoparticles are efficient supports which can facilitate the isolation and recycling of expensive catalysts from the reaction media.<sup>47,48</sup>

In this research, an advance in the context of synthetic methodology towards the mentioned class of biologically important materials is presented using a new magnetic inorganic-organic nanohybrid material,  $H_6P_2W_{18}O_{62}$ /pyridino- $Fe_3O_4$ . This new environmentally benign, heterogeneous, and highly reusable catalyst showed very good catalytic activity towards condensation of  $\beta$ -naphthol with different aldehydes and benzamide (Scheme 1).

The condensation of a mixture of benzaldehyde (1 mmol) with  $\beta$ -naphthol (1 mmol) and benzamide (1.2 mmol) in the presence of HPA/TPI- $Fe_3O_4$  (20 mg) was carried out at 100 °C for 30 min under solvent-free conditions (Scheme 1). The reaction proceeded smoothly and gave the corresponding amidoalkyl-naphthol as the sole product in 92% yield.

## 2 Experimental

### 2.1 Materials and methods

All starting materials and solvents were commercially available and were used as received. All products were identified by comparison of their spectral and physical data with those previously reported.<sup>49–51</sup> Progress of the reactions was monitored by thin-layer chromatography (TLC). Melting points were recorded on a Bamstead electrothermal type 9200 melting point apparatus. Ultraviolet-visible spectra were recorded on a Shimadzu Model UV-2550 spectrophotometer. Infrared spectra were recorded (KBr pellets) on an 8700 Shimadzu Fourier Transform spectrophotometer.  $^1H$  and  $^{13}C$  NMR spectra were recorded on a Bruker AVANCE 300-MHz instrument using TMS as internal reference. X-ray diffraction patterns were obtained on a STOE diffractometer with  $Cu K\alpha$  radiation at 60 keV and 15 mA with a scanning rate of  $3^\circ \text{ min}^{-1}$  in the  $2\theta$  range from  $5^\circ$  to  $80^\circ$ . Transmission electron microscopy (TEM) was performed on a Philips CM120 with a magnification of 160 and 200 K. For observation of morphology by TEM, the sample was dispersed in ethanol using ultrasonication for several minutes. A drop of the dispersed particles in ethanol was poured on a carbon-coated copper grid and then the grid was dried under an infrared lamp, followed by inspection in the TEM. Thermal analysis (TGA-DTA) was carried out on a Bahr STA-503 instrument in air at a heating rate of  $10^\circ \text{ C min}^{-1}$ . The heteropolyacid catalyst  $H_6P_2W_{18}O_{62}$ , was prepared and characterized according to the literature procedure as described below.<sup>52</sup>

The tungsten content in the nanohybrid catalyst was determined using inductively coupled plasma optical emission spectroscopy (ICP-OES) conducted on a Varian Vista-Pro model ICP-OES spectrometer.

### 2.2 Preparation of Wells–Dawson $H_6P_2W_{18}O_{62}\cdot 24H_2O$ acid catalyst

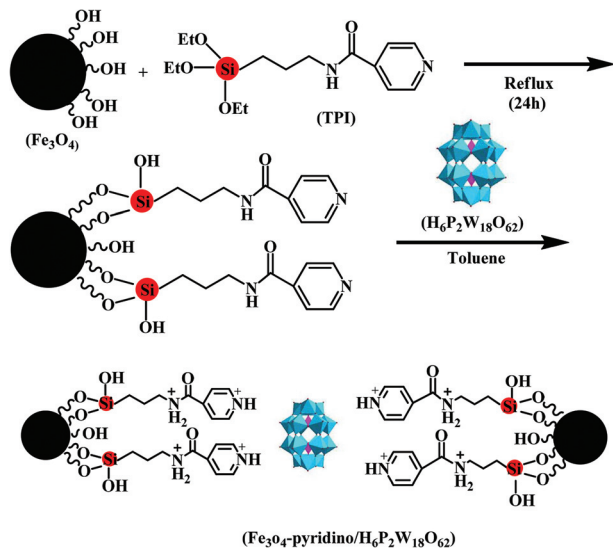
Wells–Dawson acid ( $H_6P_2W_{18}O_{62}\cdot 24H_2O$ ) was prepared from an  $\alpha/\beta$ - $K_6P_2W_{18}O_{62}\cdot 10H_2O$  isomer mixture as described before.<sup>53–55</sup> Concentrated  $H_3PO_4$  in a 4 : 1 acid : salt ratio was added to the boiling aqueous solution of  $Na_2WO_4\cdot 2H_2O$  and the mixture was kept boiling in a reflux system for 8 h. The salt was precipitated by adding KCl, then purified by re-crystallization and cooled overnight to 5 °C. The product consisted of a mixture of the  $\alpha$ - and  $\beta$ -isomers, was filtered, washed, and then vacuum-dried for 8 h. The acid was obtained from an aqueous solution of  $\alpha/\beta$   $K_6P_2W_{18}O_{62}\cdot 10H_2O$  salt, which was treated with ether and concentrated HCl (37%) solution. The acid so released formed an addition compound with ether, which allows it to be separated from the solution. After obtaining the ether solution with the acid, the ether was eliminated by flowing dry air and the remaining solution was placed in a vacuum-desiccator until crystallization.

### 2.3 Synthesis of $Fe_3O_4$ and pyridine-functionalized $Fe_3O_4$ nanoparticles (TPI- $Fe_3O_4$ )

$Fe_3O_4$  nanoparticles were synthesized according to a previously reported procedure.<sup>56</sup> 10.4 g of  $FeCl_3\cdot 6H_2O$  and 4.0 g of  $FeCl_2\cdot 4H_2O$  were dissolved in 100 ml of deionized water, degassed with nitrogen gas for 15 min and heated to 80 °C. Then, 15 ml of  $NH_3$  (32% aqueous solution) was added dropwise to the solution. After 15 min, the solid product was separated by a magnet and washed three times with NaCl (0.1 M) solution. The identity of the prepared nanoparticles was confirmed by FTIR and X-ray powder diffraction. For the preparation of pyridine-functionalized  $Fe_3O_4$ , 1.0 g of  $Fe_3O_4$  was suspended in 50 ml toluene, and the mixture was stirred for 1 h. Then, 2 ml of TPI was added and the mixture was refluxed for 24 h. The black solid was removed by filtration and washed with toluene and ethanol, then dried at room temperature. The synthesized  $Fe_3O_4$  and pyridine-functionalized material (TPI- $Fe_3O_4$ ) were characterized by FTIR spectroscopy, X-ray diffraction, thermal analysis (TGA/DTA), and transmission electron microscopy (TEM).

### 2.4 Immobilization of Wells–Dawson diphosphooctadecatungstic acid on TPI- $Fe_3O_4$

For the immobilization of  $H_6P_2W_{18}O_{62}\cdot 24H_2O$  on TPI- $Fe_3O_4$ , 50 ml of methanol solution containing 0.3 g of  $H_6P_2W_{18}O_{62}\cdot 24H_2O$  was added to freshly prepared TPI- $Fe_3O_4$  (0.6 g) and the mixture was refluxed for 3 h. Then, the heterogeneous catalyst was filtered off and extracted in a Soxhlet extractor using methanol as solvent for 12 h and thereafter was dried at 105 °C in a vacuum oven. The amount of  $H_6P_2W_{18}O_{62}\cdot 24H_2O$  loading on TPI- $Fe_3O_4$  was found  $0.02 \text{ mmol g}^{-1}$ , as determined by ICP-OES after digestion in aqua regia, and this was



**Scheme 2** A schematic for the preparation of HPA/TPI-Fe<sub>3</sub>O<sub>4</sub> nanocatalyst.

confirmed by UV-vis analysis with  $\pm 5\%$  uncertainty. The functionalized TPI-Fe<sub>3</sub>O<sub>4</sub> supported by H<sub>6</sub>P<sub>2</sub>W<sub>18</sub>O<sub>62</sub>·24H<sub>2</sub>O did not leach significantly after prolonged contact with aqueous solution as confirmed by UV-vis. Therefore, *N*-[3-(triethoxysilyl)propyl]isonicotinamide (TPI) linker is a suitable agent for the immobilization process and provided covalent anchoring of the heteropolyacid onto the functionalized supporting material. A schematic for the preparation of HPA/TPI-Fe<sub>3</sub>O<sub>4</sub> nanocatalyst is shown in Scheme 2.

## 2.5 General procedure for the preparation of substituted 1-amidoalkyl-2-naphthols

In a typical reaction, a mixture of  $\beta$ -naphthol (1.0 mmol), aldehyde (1 mmol), benzamide (1.2 mmol), and H<sub>6</sub>P<sub>2</sub>W<sub>18</sub>O<sub>62</sub>/pyridino-Fe<sub>3</sub>O<sub>4</sub> (20 mg) in a small test tube equipped with a condenser, was heated to 100 °C in an oil bath for the required time. After completion of the reaction (monitored by TLC), the mixture was cooled to 25 °C, boiling ethanol was added and the mixture was stirred for 5 min. The catalyst was recovered by using an external magnet. Then, the solution was cooled to room temperature and the resulting solid was filtered off and re-crystallized from aqueous ethanol 15%.

## 2.6 Spectral data for some selected 1-amidoalkyl-2-naphthols<sup>16,21,25,26</sup>

***N*-(1-(2-Hydroxynaphthalen-1-yl)-3-phenylallyl)benzamide.** White solid, m.p. 234 °C, <sup>1</sup>H NMR (DMSO-d<sub>6</sub>):  $\delta$  = 7.08 (d, 1H), 7.17 (d, 1H), 7.21 (m, 4H), 7.41 (m, 3H), 7.75 (m, 3H), 8.07 (d, 1H), 9.01 (d, 1H), 10.43 (s, 1H). <sup>13</sup>C NMR (DMSO-d<sub>6</sub>):  $\delta$  = 48.15, 123.51, 127.61, 128.30, 131.27, 132.47, 133.60, 135.81, 137.28, 141.84, 158.24, 165.54. Anal. Calcd: C, 82.30; H, 5.58; N, 3.69. Found: C, 82.27; H, 5.55; N, 3.66.

***N*-(1-(2-Hydroxynaphthalen-1-yl)-3-phenylpropyl)benzamide.** White solid, m.p. 158 °C, <sup>1</sup>H NMR (DMSO-d<sub>6</sub>):  $\delta$  = 2.04 (m, 2H), 2.74 (t, 2H), 5.98 (d, 1H), 7.13–7.24 (m, 6H), 7.40–7.47

(m, 4H), 7.66–7.82 (m, 4H), 8.02 (d, 1H), 8.66 (d, 1H), 10.16 (s, 1H). <sup>13</sup>C NMR (DMSO-d<sub>6</sub>):  $\delta$  = 32.46, 35.60, 46.70, 118.59, 119.62, 122.38, 125.66, 126.22, 126.96, 127.33, 128.181, 28.26, 128.35, 128.45, 128.52, 131.13, 132.02, 134.63, 141.68, 152.90, 165.55. Anal. Calcd: C, 81.86; H, 6.08; N, 3.67. Found: C, 81.86; H, 5.98; N, 3.52.

***N*-[4-Nitrophenyl-(2-hydroxynaphthalen-1-yl)-methyl]benzamide.** FT-IR (neat) = 3420, 3062, 1627, 1572, 1534, 1489, 1347, 1271, 1026, 942, 822, 750 cm<sup>-1</sup>. <sup>1</sup>H NMR (DMSO-d<sub>6</sub>):  $\delta$  = 7.25 (m, 8H), 7.47 (t, *J* = 6.4 Hz, 3H), 7.53 (d, *J* = 6.8 Hz, 1H), 7.82 (m, 4H), 8.07 (d, *J* = 8 Hz, 1H), 9.03 (d, *J* = 8 Hz, 1H), 10.34 (br, s, 1H) ppm. <sup>13</sup>C NMR (DMSO-d<sub>6</sub>):  $\delta$  = 49.51, 117.86, 119.03, 123.11, 123.25, 123.86, 127.46, 127.91, 128.03, 128.90, 129.19, 130.45, 132.05, 132.75, 134.44, 146.61, 150.76, 153.94, 166.77.

***N*-[2-(2-Hydroxynaphthalen-1-yl)-phenylmethyl]benzamide.** White solid, m.p. 235.1–237.5 °C, <sup>1</sup>H NMR (DMSO-d<sub>6</sub>)  $\delta$  = 10.34 (br, s, 1H), 8.17–8.11 (m, 6H), 7.92–7.87 (m, 5H), 7.40 (br, s, 1H), 7.20–7.14 (m, 5H), 6.07 (s, 1H); <sup>13</sup>C NMR (DMSO-d<sub>6</sub>)  $\delta$  = 169.5, 153.4, 148.2, 145.2, 134.8, 133.4, 132.8, 132.2, 130.8, 130.3, 129.7, 128.4, 128.1, 127.7, 127.1, 123.8, 122.6, 122.6, 121.0, 119.3, 118.1, 49.7; Anal. Calcd: C, 81.56; H, 5.42; N, 3.96. Found: C, 81.73; H, 5.51; N, 3.90.

***N*-[4-Tolyl-(2-hydroxynaphthalen-1-yl)-methyl]benzamide.** Light yellow solid, m.p. 207.5–209.8 °C, <sup>1</sup>H NMR (DMSO-d<sub>6</sub>, TMS)  $\delta$  = 9.91 (br, s, 1H), 8.04–7.98 (m, 6H), 7.63 (br, s, 1H), 7.23–7.14 (m, 9H), 6.07 (s, 1H), 1.91 (s, 3H); <sup>13</sup>C NMR (DMSO-d<sub>6</sub>)  $\delta$  = 167.8, 153.1, 143.3, 139.5, 134.7, 132.9, 129.1, 128.8, 128.2, 126.3, 125.5, 123.4, 122.6, 119.4, 118.1, 48.7, 20.3; Anal. Calcd: C, 81.72; H, 5.76; N, 3.81. Found: C, 81.53; H, 6.11; N, 3.87.

***N*-[4-Chlorophenyl-(2-hydroxynaphthalen-1-yl)-methyl]benzamide.** Off white solid, m.p. 179.0–181.6 °C, *R*<sub>f</sub> = 0.24 (50% AcOEt-hexane); <sup>1</sup>H NMR (400 MHz, DMSO-d<sub>6</sub>, TMS)  $\delta$  = 10.06 (br, s, 1H, OH), 8.06–7.97 (m, 6H, Ar-H), 7.43 (br, s, 1H, NH), 7.28–7.23 (m, 4H, Ar-H), 7.07–7.01 (m, 5H, Ar-H), 6.12 (s, 1H, CH); <sup>13</sup>C NMR (100 MHz, DMSO-d<sub>6</sub>)  $\delta$  = 165.0, 153.3, 138.7, 134.1, 132.5, 132.1, 131.2, 130.6, 129.7, 128.4, 128.2, 128.0, 127.8, 127.3, 126.7, 126.2, 122.9, 122.4, 118.7, 116.6, 48.9; IR (KBr pellets)  $\nu_{\max}$  (cm<sup>-1</sup>) 3440 (N-H), 3325 (O-H), 3070 (C-H), 1644 (C=O); *m/z* (GC-MS) 387.10 [M<sup>+</sup>]. Anal. Calcd for C<sub>24</sub>H<sub>18</sub>ClNO<sub>2</sub>: C, 74.32; H, 4.68; N, 3.61. Found: C, 74.26; H, 4.60; N, 3.86.

***N*-[2-(2-Hydroxynaphthalen-1-yl)-(4-hydroxyphenyl)methyl]benzamide.** Light brown solid, m.p. 191.3–193.3 °C, <sup>1</sup>H NMR (DMSO-d<sub>6</sub>)  $\delta$  = 11.24 (br, s, 1H), 8.94 (br, s, 1H), 8.11–8.05 (m, 6H), 7.81–7.76 (m, 4H), 7.21–7.15 (m, 5H), 6.79 (s, 1H); <sup>13</sup>C NMR (DMSO-d<sub>6</sub>)  $\delta$  = 169.6, 156.4, 152.4, 149.2, 144.7, 139.2, 134.5, 132.5, 132.1, 130.0, 129.6, 129.2, 128.8, 128.1, 127.9, 127.1, 125.2, 124.4, 122.9, 122.2, 120.8, 119.3, 50.3; IR (KBr pellets)  $\nu_{\max}$  (cm<sup>-1</sup>) 3488 (N-H), 3366 (O-H), 2955 (C-H), 1655 (C=O); Anal. Calcd: C, 78.03; H, 5.18; N, 3.79. Found: C, 77.67; H, 5.22; N, 4.08.

***N*-[1-(2-Hydroxynaphthalen-1-yl)butyl]benzamide.** White solid, m.p. 240.1–242.7 °C, <sup>1</sup>H NMR (DMSO-d<sub>6</sub>)  $\delta$  = 10.08 (br, s, 1H), 8.11–8.05 (m, 6H), 7.83–7.79 (m, 5H), 7.31 (br, s, 1H), 6.34

(t,  $J = 6.5$  Hz, 1H), 2.15 (s, 3H), 1.84–1.78 (m, 1H), 1.39–1.33 (m, 1H), 0.97 (t,  $J = 6.5$  Hz, 3H);  $^{13}\text{C}$  NMR (DMSO- $d_6$ )  $\delta = 162.7$ , 155.3, 148.1, 144.6, 139.7, 139.2, 135.1, 133.7, 132.4, 129.3, 128.8, 128.3, 127.7, 126.2, 125.3, 122.8, 119.6, 118.4, 48.7, 36.3, 19.4, 13.3; IR (KBr pellets)  $\nu_{\text{max}}$  ( $\text{cm}^{-1}$ ) 3469 (N–H), 3239 (O–H), 3010 (C–H), 1659 (C=O); Anal. Calcd: C, 78.97; H, 6.63; N, 4.39. Found: C, 79.11; H, 6.92; N, 4.45.

### 3 Results and discussion

The design and preparation of multifunctional materials bearing different types of active sites have attracted more and more attention from chemical engineers.<sup>57–62</sup> Therefore, various kinds of supports, including organic and inorganic materials,<sup>63–66</sup> have been employed in the field of catalytic sciences to show unique properties in different catalytic reactions.<sup>67–69</sup> Generally, nanoparticles have been applied as efficient supports for the preparation of functionalized materials because of nano-effects. But, the separation processes becomes a challenge, because nanoparticles are often readily dispersed in the liquid media. This issue may be overcome by using magnetic materials; they offer the advantage of being magnetically separable by using an external magnetic field. Amongst various metal oxide nanoparticles which have emerged as potential heterogeneous catalysts,  $\text{Fe}_3\text{O}_4$  nanoparticles arguably have attracted the most attention. The reason would be due to the ease of handling, ease of recovery, as well as the high catalytic activity of  $\text{Fe}_3\text{O}_4$  nanoparticles in various organic transformations.<sup>48,70</sup>

In continuation of our recent activities on the utilization of new organic–inorganic nanohybrid heterogeneous catalysts in different areas of organic synthesis,<sup>71,72</sup> a new environmentally benign and highly reusable magnetic nanocatalyst is introduced for the efficient synthesis of various substituted 1-amidoalkyl-2-naphthols under solvent-free conditions.

#### 3.1 Structural characterization of the magnetic inorganic–organic nanohybrid material HPA/TPI- $\text{Fe}_3\text{O}_4$

**3.1.1 UV-vis spectroscopy.** The UV-vis spectrum of the Wells–Dawson heteropolyacid shows two types of ligand→metal charge-transfer bands originating from different oxygen atoms. The highest energy absorption band at about 220 nm has been assigned to the  $\text{O}_d \rightarrow \text{W}$  charge-transfer band due to the terminal oxygen atoms. Other weak bands at  $\sim 260$  and  $\sim 310$  nm are characteristic bands for diphosphooctadecatungstic acid<sup>73</sup> and have been attributed to the  $\text{O}_b \rightarrow \text{W}$  or  $\text{O}_c \rightarrow \text{W}$  charge-transfer bands of the bridge-oxygen atoms.

To determine the optimum refluxing time that is required for  $\text{Fe}_3\text{O}_4$ -TPI to adsorb HPA from the impregnating solution, and also to determine the extent of HPA which can be loaded on the support (as an ancillary method along with ICP analysis), 0.2 g  $\text{Fe}_3\text{O}_4$ -TPI was suspended in a 40 ml methanol solution of HPA with an initial concentration 2500 ppm. The suspension was refluxed and at different refluxing time ranging from 1 to 240 minutes, adsorption studies were

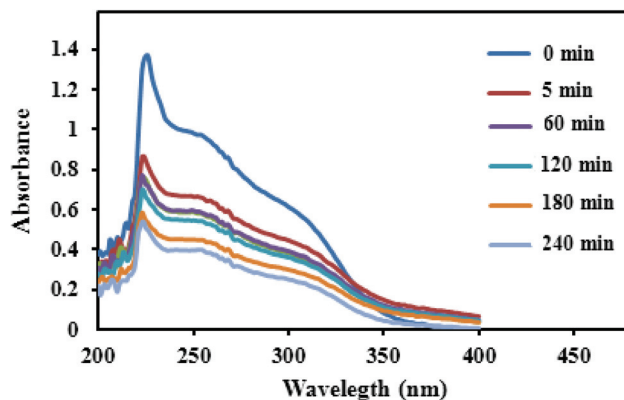


Fig. 1 Stacked plot of UV-vis spectral changes after addition of  $\text{H}_6\text{P}_2\text{W}_{18}\text{O}_{62}$  to TPI- $\text{Fe}_3\text{O}_4$  under aerobic conditions with time.

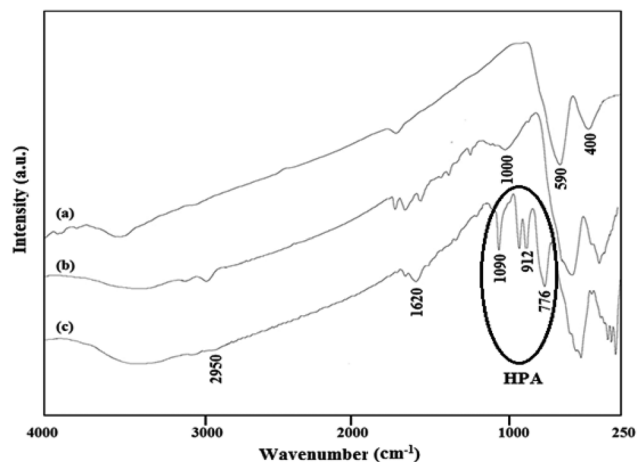


Fig. 2 FTIR spectra of (a)  $\text{Fe}_3\text{O}_4$ , (b)  $\text{Fe}_3\text{O}_4$ -TPI, and (c)  $\text{H}_6\text{P}_2\text{W}_{18}\text{O}_{62}/\text{Fe}_3\text{O}_4$ -TPI.

recorded for solutions after removing the solid catalyst by an external magnetic field. As Fig. 1 shows, the main adsorption has occurred during the first three hours and there was no significant change in it even after one hour more. By comparison with standard solutions, after 180 min refluxing, the heteropolyacid concentration had declined to 1400 ppm which corresponded to  $0.025 \text{ mmol g}^{-1}$  loading of HPA on the support.

**3.1.2 FTIR spectroscopy.** FTIR spectroscopy was applied to characterize the composition of the  $\text{Fe}_3\text{O}_4$ -TPI nanoparticles. *N*-[3-(Triethoxysilyl)propyl]isonicotinamide (TPI) was used to modify the  $\text{Fe}_3\text{O}_4$  nanoparticles in refluxing toluene. The TPI was anchored onto the surface of  $\text{Fe}_3\text{O}_4$  by condensation of the surface hydroxyl groups of the mesoporous material with the ethoxy groups of TPI as illustrated in Scheme 2. Incorporation of the linker into the surface of  $\text{Fe}_3\text{O}_4$  was confirmed by FTIR (Fig. 2). The absorbance at about  $590 \text{ cm}^{-1}$  is ascribed to  $\text{Fe}^{2+}-\text{O}^{2-}$ , which is consistent with the reported infrared spectra for spinel  $\text{Fe}_3\text{O}_4$ .<sup>74</sup> The detection of weak characteristic stretching vibrations of pyridine at  $1550\text{--}1650 \text{ cm}^{-1}$  and the

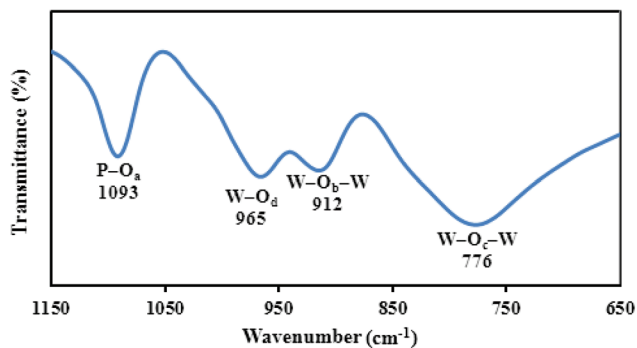


Fig. 3 The fingerprinting IR bands of  $H_6P_2W_{18}O_{62}$  with the Wells-Dawson structure.

appearance of shoulders at 2900–3000  $cm^{-1}$  in the FTIR spectrum indicated grafting of TPI group on the surface of  $Fe_3O_4$  nanoparticles. Furthermore, the Si–O–Fe, Fe–O, and Fe–O–H stretching vibration bands of  $Fe_3O_4$  nanoparticles were detected at 1150, 950, and  $>3200$   $cm^{-1}$ , respectively. The broad band in the region 3500–3700  $cm^{-1}$  can be attributed to the symmetrical stretching vibration modes of the adsorbed water molecules.

The Wells–Dawson structure of  $H_6P_2W_{18}O_{62}$  consists of two half units composed of a central  $PO_4$  tetrahedron surrounded by nine  $WO_6$  octahedra. Therefore, the  $H_6P_2W_{18}O_{62}$  structure involves four kinds of oxygen atoms. The first is P–O<sub>a</sub> in which the oxygen atom connects with the tungsten atom, the second is W–O<sub>b</sub>–W oxygen bridges (corner-sharing oxygen bridges between different  $W_3O_{13}$  groups), the third is W–O<sub>c</sub>–W oxygen bridges (edge-sharing oxygen bridge within  $W_3O_{13}$  groups), and the last is W–O<sub>d</sub> terminal oxygen atoms. As shown in Fig. 3, the four characteristic bands of  $H_6P_2W_{18}O_{62}$  appeared, *i.e.*  $\nu_{as}(W-O_d)$ : 965  $cm^{-1}$ ;  $\nu_{as}(W-O_b-W)$ : 912  $cm^{-1}$ ;  $\nu_{as}(W-O_c-W)$ : 776  $cm^{-1}$  and  $\nu_{as}(P-O_a)$ : 1093  $cm^{-1}$ .<sup>52,75</sup> The intense band at 1090  $cm^{-1}$  is assigned to the stretching mode of the P–O species that is considered as the fingerprint of the Wells–Dawson heteropolyanion. The vibration bands at 912 and 776  $cm^{-1}$  were assigned to the ‘inter’ and ‘intra’ W–O–W bridges, respectively. The IR spectrum of  $H_6P_2W_{18}O_{62}/TPI-Fe_3O_4$  nanoparticles possessed a distinct band with shoulders about 1030  $cm^{-1}$ , confirming a strong interaction of the pyridine-modified  $Fe_3O_4$  with the heteropolyacid. Moreover, observation of the fingerprinting IR bands of the Wells–Dawson structure in the 800–1000  $cm^{-1}$  region proved loading of  $H_6P_2W_{18}O_{62}$  onto the surface of TPI- $Fe_3O_4$ .

**3.1.3 X-ray diffraction analysis.** The crystalline nature of  $H_6P_2W_{18}O_{62}/Fe_3O_4$ -TPI nanoparticles was demonstrated by XRD and along with X-ray diffraction patterns of  $Fe_3O_4$  and TPI- $Fe_3O_4$  as shown in Fig. 4. The positions and relative intensities of all diffraction peaks matched well with those from the JCPDS card (75-1610) for magnetite and the sharp, strong peaks confirmed that the modified magnetic nanoparticles were well crystallized, which suggested that the  $Fe_3O_4$  core particles were well retained under modification with TPI. The XRD pattern of the  $Fe_3O_4$  exhibited the (220), (311), (400),

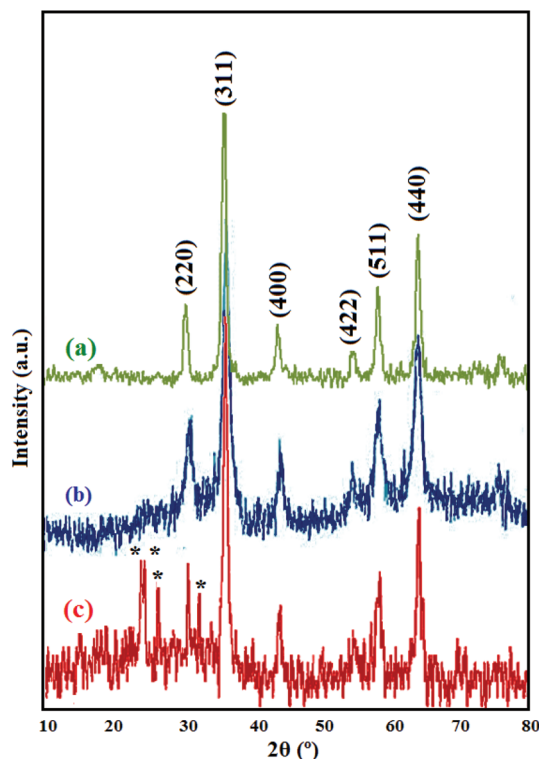


Fig. 4 X-ray diffraction patterns of  $Fe_3O_4$  (a), TPI- $Fe_3O_4$  (b), and HPA/TPI- $Fe_3O_4$  (c).

(422), (511) and (440) reflections which is consistent with the standard  $Fe_3O_4$  crystal with the spinel structure.<sup>56a</sup> For the XRD of the  $Fe_3O_4$ -TPI nanoparticles (Fig. 4b), compared to Fig. 4a, the typical diffraction peaks were similar to those of the unfunctionalized core–shell  $Fe_3O_4$  microspheres though the intensities of the main peaks decreased marginally, which revealed that the crystal structure of the  $Fe_3O_4$  cores was still well-maintained after the introduction of organic functional groups. The position and relative intensities of all diffraction peaks match well with the standard magnetite peaks. Therefore, the spinel structure of  $Fe_3O_4$  is retained after functionalization with TPI and immobilization of HPA onto TPI- $Fe_3O_4$ . In addition, the sample is crystalline and  $Fe_3O_4$  with a spinel structure is the only obtained phase together with some additional peaks, indicated by asterisks, associated with the Well–Dawson structured  $H_6P_2W_{18}O_{62}$ .<sup>56b</sup>

**3.1.4 TEM studies.** In this work, the size and morphology of the  $H_6P_2W_{18}O_{62}/Fe_3O_4$ -TPI nanoparticles were investigated by TEM and the result is shown in Fig. 5. The micrograph illustrates that the  $Fe_3O_4$  core was coated with a TPI shell uniformly, and particles have semi-spherical morphology with narrow size distributions and an average diameter of approximately 10 nm.

**3.1.5 Thermal analysis.** The thermal stability of HPA/TPI- $Fe_3O_4$  nanoparticles was investigated by carrying out TGA–DTA analysis (Fig. 6). The DTA profile exhibited a broad endothermic peak from room temperature to 200 °C which is attributed to the elimination of adsorbed water molecules.

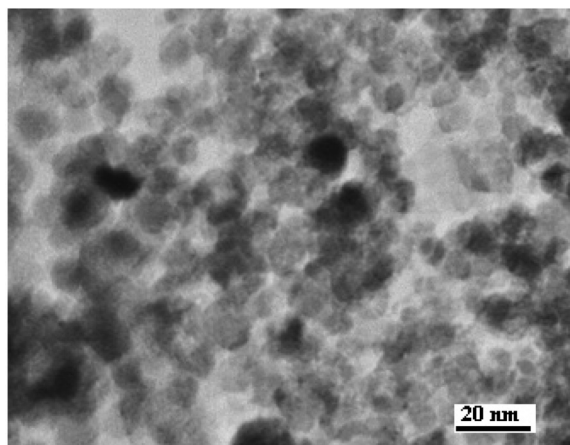


Fig. 5 TEM micrograph of nanohybrid catalyst  $\text{H}_6\text{P}_2\text{W}_{18}\text{O}_{62}/\text{Fe}_3\text{O}_4\text{-TPI}$ .

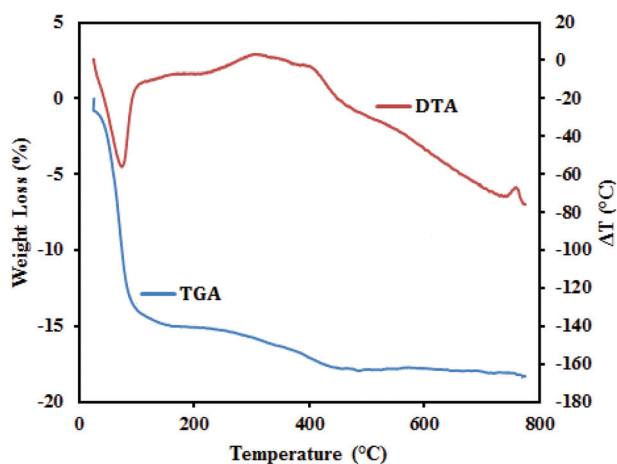


Fig. 6 TGA and DTA curves of  $\text{HPA/TPI-Fe}_3\text{O}_4$ .

A weight loss occurred between 200 °C and 500 °C which is accompanied by a broad exothermic peak between 350 °C and 450 °C in the DTA curve, corresponding to the oxidative decomposition of the organic part *N*-[3-(triethoxysilyl)propyl]-isonicotinamide (TPI). Furthermore, according to thermal analysis, the prepared nanocatalyst was stable up to 200 °C.

### 3.2 Effect of catalyst concentration on the condensation reaction

The catalytic efficiency of the  $\text{HPA/TPI-Fe}_3\text{O}_4$  heterogeneous catalytic system was studied for the preparation of  $\alpha$ -amidoalkyl- $\beta$ -naphthol with various amounts of catalyst (Table 1). A test reaction using  $\beta$ -naphthol, benzaldehyde, and benzamide at 100 °C without catalyst was performed in order to establish the real effectiveness of the catalyst. It was found that no conversion to product was obtained even after 3 h of heating. In order to evaluate the appropriate catalyst loading, a model reaction using  $\beta$ -naphthol, benzaldehyde, and benzamide was carried out using 5–100 mg of  $\text{HPA/TPI-Fe}_3\text{O}_4$ . It was found that 5 mg of catalyst, incorporating 1.6 mg of  $\text{H}_6\text{P}_2\text{W}_{18}\text{O}_{62}$ , afforded 56% of product after 1 h. This finding

Table 1 Effect of catalyst amount on the condensation of  $\beta$ -naphthol with benzaldehyde and benzamide under solvent free conditions<sup>a</sup>

Entry	HPA/TPI- $\text{Fe}_3\text{O}_4$ (mg)	$\text{H}_6\text{P}_2\text{W}_{18}\text{O}_{62}$ (mg)	Time (min)	Yield (%)
1	0	0	180	9
2	5	0.45	60	56
3	10	0.9	60	74
4	15	1.35	45	77
5	20	1.8	30	92
6	100	9	20	93

<sup>a</sup> A mixture of aldehyde (1 mmol),  $\beta$ -naphthol (1 mmol), benzamide (1.2 mmol) and the catalyst was stirred at 100 °C for the appropriate time. Progress of the reaction was monitored with TLC. Work-up was carried out as described in the experimental section.

revealed that the heterogeneous catalyst exhibited high catalytic activity in the desired transformation. Higher amounts of the catalyst (>20 mg) neither increased, nor lowered the yield%. Therefore, 20 mg of catalyst was found to be the optimal quantity and sufficient to push the reaction forward.

### 3.3 Studying the catalytic activity of the ingredients comprising the organic-inorganic hybrid nanomaterial

Table 2 compares the catalytic activity of  $\text{HPA/TPI-Fe}_3\text{O}_4$  with  $\text{H}_6\text{P}_2\text{W}_{18}\text{O}_{62}$ ,  $\text{TPI-Fe}_3\text{O}_4$ , and  $\text{Fe}_3\text{O}_4$  dispositions, separately, in the preparation of  $\alpha$ -amidoalkyl- $\beta$ -naphthol under the standard reaction conditions. 6.4 mg of  $\text{H}_6\text{P}_2\text{W}_{18}\text{O}_{62}$  catalyst led to 42% of the desired product after 40 min (entry 1); whereas, 20 mg of the inorganic-organic hybrid material  $\text{HPA/TPI-Fe}_3\text{O}_4$ , which includes only 6.4 mg of the heteropolyacid achieved 92% yield after a short time of 30 min (entry 4). The free carrier material ( $\text{Fe}_3\text{O}_4$ ) and the modified material  $\text{TPI-Fe}_3\text{O}_4$  were also catalytically active; findings revealed that the first led to 33% of product after 60 min and the latter produced 38% of product after 30 min (entries 2 and 3, respectively). Although the components of the composite material showed a little catalytic activity,  $\text{HPA/TPI-Fe}_3\text{O}_4$  gave the best result in the desired organic transformation (entry 4). Clearly, immobilizing the heteropolyacid onto the modified solid material  $\text{TPI-Fe}_3\text{O}_4$  drastically increased its catalytic activity toward the condensation reaction.

### 3.4 Effect of organic solvent on the condensation reaction

The need to reduce the amount of toxic waste and byproducts arising from chemical processes requires increasing emphasis

Table 2 Studying the catalytic activity of  $\text{H}_6\text{P}_2\text{W}_{18}\text{O}_{62}$ ,  $\text{TPI-Fe}_3\text{O}_4$ , and  $\text{Fe}_3\text{O}_4$  in the preparation of  $\alpha$ -amidoalkyl- $\beta$ -naphthol<sup>a</sup>

Entry	Catalyst	Catalyst (mg)	Time (min)	Yield (%)
1	HPA	6.4	40	42
2	$\text{Fe}_3\text{O}_4$	20	60	33
3	$\text{TPI-Fe}_3\text{O}_4$	20	30	38
4	$\text{HPA/TPI-Fe}_3\text{O}_4$	20	30	92

<sup>a</sup> Reaction conditions are described below Table 1.

**Table 3** Effect of different solvents on the synthesis of  $\alpha$ -amidoalkyl- $\beta$ -naphthol in the presence of HPA/TPI- $\text{Fe}_3\text{O}_4$  at 60 °C<sup>a</sup>

Entry	Solvent	Boiling point (°C)	Time (min)	Yield (%)
1	H <sub>2</sub> O	100	120	17
2	CH <sub>3</sub> CN	81	120	83
3	CH <sub>3</sub> OH	65	120	41
4	C <sub>2</sub> H <sub>5</sub> OH	78	120	57
5	CHCl <sub>3</sub>	61	120	62
6	ClCH <sub>2</sub> CH <sub>2</sub> Cl	83	120	86
7	—	—	30	92

<sup>a</sup> Reaction conditions are as described below Table 1 (except for reaction temperature). 1.0 ml solvent was used.

on the use of less toxic and environmentally compatible materials in the design of new synthetic methods.<sup>76</sup> One of the most promising approaches is focused on the use of solvent-less conditions.

We examined the target transformation under similar conditions in different solvents. Solvents such as water, ethanol, methanol, acetonitrile, 1-2 dichloroethane, and chloroform were screened in a model reaction of  $\beta$ -naphthol with benzaldehyde and benzamide in the presence of 0.02 g of HPA/pyridino- $\text{Fe}_3\text{O}_4$  nanoparticles (Table 3). This study was conducted at a fixed temperature, 60 °C, in all cases. The solvent influenced the catalytic performance; however, the best yield was picked up under the solvent free condition (Table 3, entry 7). Almost all the reactions were less efficient in the presence of solvent than in its absence, considering the reaction time and yield%. Acetonitrile and 1-2 dichloroethane resulted in better performance amongst all the examined solvents. The target multi-component reaction under solvent-free conditions is fascinating, since it involves the best reaction medium with “no medium”.

### 3.5 Effect of temperature on the multi-component condensation reaction

The effect of temperature on the preparation of  $\alpha$ -amidoalkyl- $\beta$ -naphthol was investigated in the presence of HPA/TPI- $\text{Fe}_3\text{O}_4$  nanoparticles (0.02 g) under solvent-free conditions (Fig. 7). The yield of the desired product was enhanced by increasing

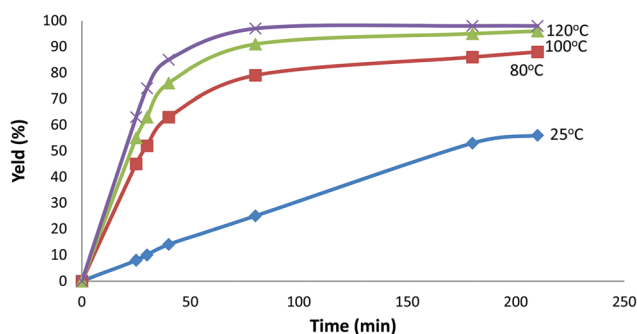


**Fig. 7** Effect of reaction temperature on the condensation of  $\beta$ -naphthol, benzaldehyde, and benzamide catalyzed by HPA/TPI- $\text{Fe}_3\text{O}_4$  under solvent free conditions.

the temperature from 25 to 120 °C. At temperatures lower than 100 °C, the reaction did not proceed efficiently and most of the initial substances remained intact.

### 3.6 Synthesis of different $\alpha$ -amidoalkyl- $\beta$ -naphthols in the presence of HPA/TPI- $\text{Fe}_3\text{O}_4$ under solvent free conditions

Multi-component reactions have drawn high efforts in recent years owing to their exceptional synthetic efficiency, intrinsic atom economy, procedural simplicity, and reducing the number of steps, energy consumption, and waste production. The multi-component, one-pot condensation of  $\beta$ -naphthol, aromatic or aliphatic aldehydes, and benzamide constitutes a valuable approach for the creation of structurally related drug-like compounds.

The non-toxicity and chemical stability of the new synthesized organic-inorganic hybrid material HPA/TPI- $\text{Fe}_3\text{O}_4$  is amongst the most crucial characteristics of this super paramagnetic iron oxide nanocatalyst. The generality of the protocol was confirmed by using structurally diverse aromatic and aliphatic aldehydes carrying either electron-withdrawing, electron-donating, and halogen groups on their aromatic rings in the condensation reaction and gave the desired products in high yields in short reaction times (Table 4). It was shown that aromatic aldehydes with electron withdrawing groups reacted faster than their analogues with electron releasing groups. In contrast to the previously reported methods,<sup>77–79</sup> in which aliphatic aldehydes were not transformed into the corresponding 1-amidoalkyl-2-naphthols, they were converted into the desired product in good yields in the current methodology. Findings revealed that this protocol is effective for a wide range of aldehydes. However, aliphatic aldehydes showed less reactivity toward condensation reaction than aromatic analogues.

### 3.7 Hot filtration test

In order to confirm that the catalytic activity was generated from the conjugated  $\text{Fe}_3\text{O}_4$  nanoparticles on HPA-TPI and not from leached components in the reaction mixture, a hot filtration test was carried out. In this technique, the condensation reaction was performed at 100 °C for 20 min in the presence of the  $\text{Fe}_3\text{O}_4$ -TPI/HPA magnetic nanocatalyst. At this stage, the yield of the product was 63%. The catalyst was then filtered off under hot conditions, and with the filtrate, which was obtained after separation of the catalyst after 20 min, the reaction was continued for another 20 min at the same reaction temperature. But, no corresponding increase in product yield beyond 63% was observed. This result confirmed the heterogeneous nature of the magnetic nanocatalyst in this condensation reaction and that no leaching of the heteropolyacid occurred during the course of the reaction.

### 3.8 Reusability and reproducibility of HPA/TPI- $\text{Fe}_3\text{O}_4$ nanoparticles

To investigate the reusability of the HPA/TPI- $\text{Fe}_3\text{O}_4$  nanoparticles, it was easily separated from the reaction mixture by an external magnet and washed thoroughly with chloroform.

Table 4 Synthesis of various  $\alpha$ -amidoalkyl- $\beta$ -naphthol derivatives in the presence of HPA/TPI- $\text{Fe}_3\text{O}_4$  under solvent free conditions<sup>a</sup>

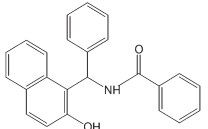
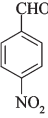
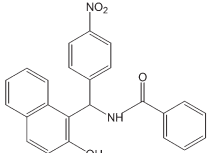
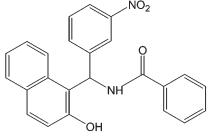
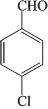
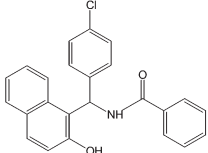
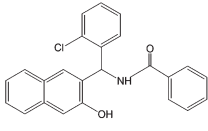
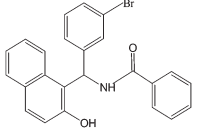
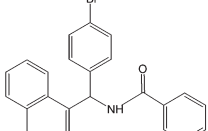
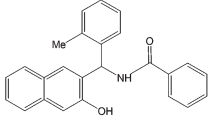
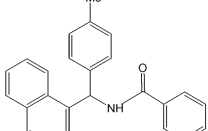
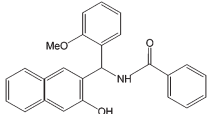
Entry	Aldehyde	Time (min)	Yield (%)	M.P. (lit. m.p.)	Product
1		30	92	235 (235–237) <sup>23</sup>	
2		25	94	237 (239–241) <sup>24</sup>	
3		30	88	239 (240–242) <sup>27</sup>	
4		30	91	177 (176–177) <sup>27</sup>	
5		35	75	286 (284–285) <sup>14</sup>	
6		35	83	230–232	
7		35	87	243–244	
8		40	85	215 (215–216) <sup>27</sup>	
9		45	88	202 (204–205) <sup>27</sup>	
10		25	61	267 (266–267) <sup>14</sup>	

Table 4 (Contd.)

Entry	Aldehyde	Time (min)	Yield (%)	M.P. (lit. m.p.)	Product
<p style="text-align: center;">R = aryl or alkyl</p>					
11		35	76	232	
12		30	87	220–223	
13		35	86	265–267	
14		25	74	234–236	
15		30	93	194 (193–194) <sup>16</sup>	
16		45	60	221 (220–221) <sup>14</sup>	
17		30	57	175–178	
18		30	50	168	
19		30	75	159 (158) <sup>26</sup>	

Table 4 (Contd.)

R = aryl or alkyl

Entry	Aldehyde	Time (min)	Yield (%)	M.P. (lit. m.p.)	Product
20		45	48	247–248	
21		60	57	235 (233–235) <sup>27</sup>	
22		30	52	237–239	
23		30	47	241 (240–242) <sup>20</sup>	
24		60	71	183	
25		25	83	236 (234) <sup>26</sup>	

<sup>a</sup> Reaction conditions are described below Table 1.

Then, the catalyst was slowly dried in air and then was activated in a vacuum oven at 80 °C for 2 h. Finally, the recycled catalyst was reused for another condensation reaction. Findings revealed the same catalytic activity as the fresh catalyst, without any loss of its activity (Fig. 8). Moreover, to ensure reproducibility of the transformation, repeated typical experiments were carried out under identical reaction conditions. The obtained yields were found to be reproducible within  $\pm 2\%$  variation.

### 3.9 Comparison of the catalytic activity of HPA/TPI-Fe<sub>3</sub>O<sub>4</sub> nanoparticles with some reported catalysts

The merit of the present heterogeneous catalyst H<sub>6</sub>P<sub>2</sub>W<sub>18</sub>O<sub>62</sub>/pyridino-Fe<sub>3</sub>O<sub>4</sub> was studied over some reported catalysts (Table 5). The reaction of  $\beta$ -naphthol with benzaldehyde and benzamide for the synthesis of  $\alpha$ -amidoalkyl- $\beta$ -naphthol was selected as a model reaction and the comparison was in terms of mol% of the catalyst, temperature, reaction time, and percentage yields. Obviously, the present new nanohybrid material is better than most of the conventional catalysts

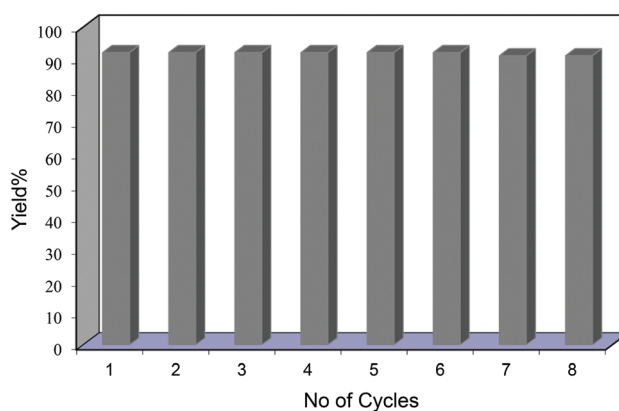


Fig. 8 Yield% as a function of reusability of H<sub>6</sub>P<sub>2</sub>W<sub>18</sub>O<sub>62</sub>/pyridino-Fe<sub>3</sub>O<sub>4</sub> nanoparticles.

mentioned. The present methodology utilized a very low amount of the supported heteropolyacid under solvent-free conditions. Although some introduced additives catalyzed the

**Table 5** Comparison of the catalytic efficiency of HPA/TPI-Fe<sub>3</sub>O<sub>4</sub> nanocatalyst with some reported catalysts for the reaction of β-naphthol with benzaldehyde and benzamide<sup>a</sup>

Entry	Catalyst	Catalyst (mol% or g); conditions	Time (h)	Yield (%)	Ref.
1	HPA/Py-Fe <sub>3</sub> O <sub>4</sub>	0.02 g; solvent-free, 100 °C	0.5	92	This work
2	H <sub>3</sub> PMo <sub>12</sub> O <sub>40</sub>	1.6 mol%; CH <sub>3</sub> COOEt, 65 °C	4	92	84
3	NKC-9	0.17 g; CHCl <sub>3</sub> , 65 °C	4	89	19
4	Mg(OOCCF <sub>3</sub> ) <sub>2</sub>	0.12 mmol; solvent-free, 100 °C	0.4	87	85
5	H <sub>3</sub> PMo <sub>12</sub> O <sub>40</sub> /SiO <sub>2</sub>	3.17 mol%; solvent-free, 120 °C	1	82	86
6	DPA	10 mol%; solvent-free, 90 °C	0.3	90	26
7	Sulfamic acid	2.5 mmol; solvent-free, 28–30 °C	4	74	16
8	1-Hexanesulfonic acid sodium salt	10 mol%; microwave-irradiation	0.1	92	87

<sup>a</sup> Mole ratio of aldehyde–2-naphthol = 1 : 1.

reaction, even though at lower temperature, they required toxic and expensive solvents, higher mol% of catalyst, and longer reaction times.

### 3.10 Effect of different catalysts on the condensation of β-naphthol with benzaldehyde and benzamide

The catalytic activity of H<sub>6</sub>P<sub>2</sub>W<sub>18</sub>O<sub>62</sub> was compared with other well-known heteropolyoxometalates and metal (non-metal) oxides in the target transformation (Table 6). The heteropolyacids introduced in Table 6 structurally divided into two important sub-classes, Keggin and Wells–Dawson. Clearly, Wells–Dawson H<sub>6</sub>P<sub>2</sub>W<sub>18</sub>O<sub>62</sub> showed higher catalytic activity than the Keggin analogue in this catalytic transformation. Amongst the examined Keggin-type heteropolyacids, H<sub>4</sub>SiW<sub>12</sub>O<sub>40</sub> showed the best reactivity; whereas, H<sub>3</sub>PMo<sub>12</sub>O<sub>40</sub> showed the lowest. Substitution of two tungsten atoms with vanadium in H<sub>3</sub>PW<sub>12</sub>O<sub>40</sub> decreased the catalytic activity, therefore, H<sub>5</sub>PW<sub>10</sub>V<sub>2</sub>O<sub>40</sub> revealed distinctly less reactivity than H<sub>3</sub>PW<sub>12</sub>O<sub>40</sub>. It is difficult to offer an exact explanation for the different catalytic reactivity pattern observed for these two structural types of heteropolyacids; since there is a complex relationship between the activity, structure, and solubility of the polyanion in the reaction medium. Changing the constituent elements of the polyanion (both hetero and addenda

atoms), affects the acid strength of the heteropolyacid as well as its catalytic activity and solubility in a wide range.<sup>80</sup>

The effects of the two organic linkers, TPI and (EtO)<sub>3</sub>Si(CH<sub>2</sub>)<sub>3</sub>NH<sub>2</sub> (named RNH<sub>2</sub>), were investigated on the catalytic efficiency of the heterogenized vanadium substituted Keggin type heteropolyacid H<sub>5</sub>PW<sub>10</sub>V<sub>2</sub>O<sub>40</sub>. Obviously, the type of solid supporting material and identity of the organic modifier strongly affected the efficiency of the fabricated catalyst. Amongst H<sub>5</sub>PW<sub>10</sub>V<sub>2</sub>O<sub>40</sub>/TPI-Fe<sub>3</sub>O<sub>4</sub> and H<sub>5</sub>PW<sub>10</sub>V<sub>2</sub>O<sub>40</sub>/RNH<sub>2</sub>-Fe<sub>3</sub>O<sub>4</sub>, the first behaved more efficiently (entries 7 and 8). As is expected, the type of supporting material played an important role; since, TPI-modified magnetite (entry 8) behaved better than zinc oxide modified with TPI (entry 6). Among various simple oxides (entries 9–14), zinc oxide behaved better and produced 23% of the desired product in a short time of 20 min. No further improvement in yield% was observed for these simple oxides after prolonging reaction times.

### 3.11 Proposed reaction pathway for the catalytic system

A plausible mechanism explaining the sequence of the events is shown in Scheme 3.<sup>81–83</sup> Presumably, the reaction proceeded *via* the *ortho*-quinonemethide (I) formed by the nucleophilic addition of β-naphthol to the carbonyl group of the aldehyde which was activated by the heteropolyacid. Finally, (I) reacts with the amide *via* Michael addition to afford the desired 1-amidoalkyl-2-naphthol.

The results displayed in Table 5, confirmed the mechanism. As indicated, electron-releasing substituents slightly decreased the yields and enhanced the reaction times (entries 9–11 and 16); whereas, aldehydes bearing electron-withdrawing substituents behaved slightly better considering yield% and reaction time. In fact, electron-releasing substituents deactivate the aldehyde to accept nucleophilic attack of β-naphthol; however, electron-withdrawing groups activate the carbonyl group of the aldehyde. These findings are in accord with the proposed mechanism.

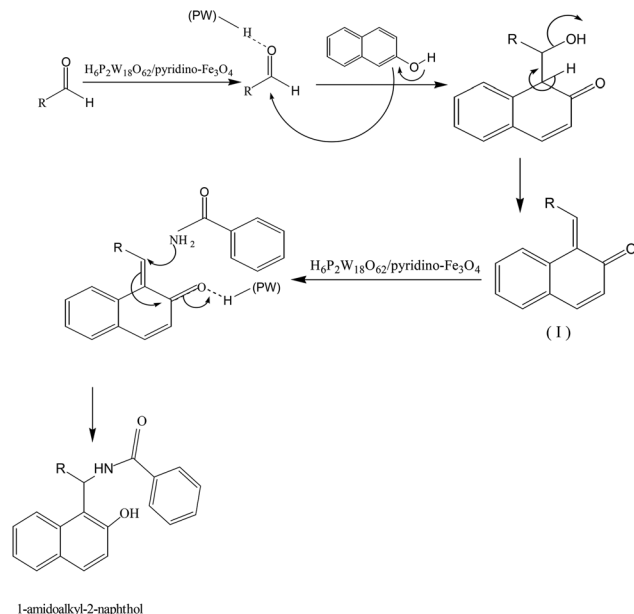
## 4 Conclusion

Heterogenization of Wells–Dawson diphosphooctadecatungstic acid (H<sub>6</sub>P<sub>2</sub>W<sub>18</sub>O<sub>62</sub>·24H<sub>2</sub>O) through immobilization on

**Table 6** Three-component condensation of β-naphthol, benzaldehyde, and benzamide in the presence of some simple and complex metal oxides

Entry	Catalyst	Time (min)	Yield (%)
1	H <sub>6</sub> P <sub>2</sub> W <sub>18</sub> O <sub>62</sub> /TPI-Fe <sub>3</sub> O <sub>4</sub>	60	74
2	H <sub>4</sub> SiW <sub>12</sub> O <sub>40</sub>	15	50
3	H <sub>3</sub> PW <sub>12</sub> O <sub>40</sub>	60	48
4	H <sub>5</sub> PW <sub>10</sub> V <sub>2</sub> O <sub>40</sub>	25	26
5	H <sub>3</sub> PMo <sub>12</sub> O <sub>40</sub>	45	24
6	H <sub>5</sub> PW <sub>10</sub> V <sub>2</sub> O <sub>40</sub> /TPI-ZnO	60	10
7	H <sub>5</sub> PW <sub>10</sub> V <sub>2</sub> O <sub>40</sub> /RNH <sub>2</sub> -Fe <sub>3</sub> O <sub>4</sub> <sup>a</sup>	60	40
8	H <sub>5</sub> PW <sub>10</sub> V <sub>2</sub> O <sub>40</sub> /TPI-Fe <sub>3</sub> O <sub>4</sub>	45	48
9	ZrO <sub>2</sub>	35	<6
10	MCM-41	120	<9
11	MCM-48	120	<9
12	SBA-15	120	12
13	KH <sub>2</sub> PO <sub>4</sub>	120	21
14	ZnO	20	23

<sup>a</sup> RNH<sub>2</sub>: (EtO)<sub>3</sub>Si(CH<sub>2</sub>)<sub>3</sub>NH<sub>2</sub>. 10 mg of catalyst was used in each case.



**Scheme 3** Proposed reaction pathway for the preparation of 1-amidoalkyl-2-naphthol mediated by HPA/TPI-Fe<sub>3</sub>O<sub>4</sub>.

modified TPI-Fe<sub>3</sub>O<sub>4</sub> and fabrication of a new organic-inorganic nanohybrid material has been the target of this research. In this powerful strategy, the active homogeneous catalyst is chemically immobilized onto the surface of the inert solid material through the action of the organic linker *N*-[3-(triethoxysilyl)propyl]isonicotinamide to overcome the potential negative aspects of catalyst leaching. The magnetic nanohybrid material H<sub>6</sub>P<sub>2</sub>W<sub>18</sub>O<sub>62</sub>/pyridino-Fe<sub>3</sub>O<sub>4</sub> was used in an environmentally friendly route for the one-pot preparation of different 1-amidoalkyl-2-naphthols. The present approach offers several promising advantages such as higher yield, easy handling, reduced reaction time, easy and green work-up, and versatility. These advantages, in general, highlight this protocol as a useful and attractive methodology, among the methods reported in the literature, for the rapid synthesis of biologically active 1-amidoalkyl-2-naphthols.

## Acknowledgements

Partial financial support from the Research Councils of Hakim Sabzevari and Shahid Beheshti universities is greatly appreciated.

## Notes and references

- 1 T. Dingermann, D. Steinhilber and G. Folkers, *Molecular Biology in Medicinal Chemistry*, Wiley-VCH, 2004.
- 2 S. Knapp, *Chem. Rev.*, 1995, **95**, 1859.
- 3 Y. Kusakabe, J. Nagatsu, M. Shibuya, O. Kawaguchi, C. Hirose and S. Shirato, *J. Antibiot.*, 1972, **2**, 44.

- 4 S. Remillard, L. I. Rebhun, G. A. Howie and S. M. Kupchan, *Science*, 1975, **189**, 1002.
- 5 G. Y. Leshner and A. R. Surrey, *J. Am. Chem. Soc.*, 1955, **77**, 636.
- 6 H. S. Mosher, M. B. Frankel and M. Gregory, *J. Am. Chem. Soc.*, 1953, **75**, 5326.
- 7 J. L. Peglion, J. Vian, B. Gourment, N. Despau, V. Audinot and M. Millan, *Bioorg. Med. Chem. Lett.*, 1997, **7**, 881.
- 8 H. Ren, S. Grady, D. Gamenara, H. Heinzen, P. Moyna, S. Croft, H. Kendrick, V. Yardley and G. Moyna, *Bioorg. Med. Chem. Lett.*, 2001, **11**, 1851.
- 9 F. Benedini, G. Bertolini, R. Cereda, G. Doná, G. Gromo, S. Levi, J. Mizrahi and A. Sala, *J. Med. Chem.*, 1995, **38**, 130.
- 10 R. D. Clark, J. M. Caroon, A. F. Kluge, D. B. Repke, A. P. Roszkowski, A. M. Strosberg, S. Baker, S. M. Bitter and M. D. Okada, *J. Med. Chem.*, 1983, **26**, 657.
- 11 H. Matsuoka, N. Ohi, M. Mihara, H. Suzuki, K. Miyamoto, N. Maruyama, K. Tsuji, N. Kato, T. Akimoto, Y. Takeda, K. Yano and T. Kuroki, *J. Med. Chem.*, 1997, **40**, 105.
- 12 S. Kantevari, S. V. N. Vuppapalapati and L. Nagarapu, *Catal. Commun.*, 2007, **8**, 1857.
- 13 Z. Karimi-Jaberi, M. Jokar and S. Z. Abbasi, *J. Chem.*, 2013, 341649.
- 14 G. C. Nandi, S. Samai, R. Kumar and M. S. Singh, *Tetrahedron Lett.*, 2009, **50**, 7220.
- 15 L. Nagarapu, M. Baseeruddin, S. Apuri and S. Kantevari, *Catal. Commun.*, 2007, **8**, 1729.
- 16 S. B. Patil, P. R. Singh, M. P. Surpur and S. D. Samant, *Ultrason. Sonochem.*, 2007, **14**, 515.
- 17 H. R. Shaterian, H. Yarahmadi and M. Ghashang, *Tetrahedron*, 2008, **64**, 1263.
- 18 S. B. Patil, P. R. Singh, M. P. Surpur and S. D. Samant, *Synth. Commun.*, 2007, **37**, 1659.
- 19 A. Li-Tao, L. Xiao-Huab, D. Fei-Qingb, J. Wen-Qingb and Z. Jian-Ping, *Chin. J. Chem.*, 2008, **26**, 2117.
- 20 G. Srihari, M. Nagaraju and M. M. Murthy, *Helv. Chim. Acta*, 2007, **90**, 1497.
- 21 V. K. Das, M. Borah and A. J. Thakur, *J. Org. Chem.*, 2013, **78**, 3361.
- 22 W. K. Su, W. Y. Tang and J. J. Li, *J. Chem. Res.*, 2008, 123.
- 23 R. R. Nagawade and D. B. Shinde, *Acta Chim. Slov.*, 2007, **54**, 642.
- 24 S. A. M. K. Ansari, N. S. Jiaprakash, D. K. S. Nagrnath, W. Pravin and D. B. Shinde, *Indian J. Chem. Technol.*, 2010, **17**, 71.
- 25 M. A. Amrollahi, F. Mirjalili and H. Emtiazi, *J. Chem. Sci.*, 2013, **125**, 561.
- 26 M. Zandi and A. R. Sardarian, *C. R. Chim.*, 2012, **15**, 365.
- 27 G. H. Mahdavinia and M. A. Bigdeli, *Chin. Chem. Lett.*, 2009, **20**, 383.
- 28 N. P. Selvam and P. T. Perumal, *Tetrahedron Lett.*, 2006, **47**, 7481.
- 29 J. Wen-Qing, A. Li-Tao and Z. Jian-Ping, *Chin. J. Chem.*, 2008, **26**, 1697.

- 30 W. K. Su, W. Y. Tang and J. J. Li, *J. Chem. Res.*, 2008, 123.
- 31 A. Khazaei, M. A. Zolfigol, A. R. Moosavi-Zare, A. Zare, A. Parhami and A. Khalafi-Nezhad, *Appl. Catal., A*, 2010, **386**, 179.
- 32 G. Srihari, M. Nagaraju and M. M. Murthy, *Helv. Chim. Acta*, 2007, **90**, 1497.
- 33 D. Kundu, A. Majee and A. Hajra, *Catal. Commun.*, 2010, **11**, 1157.
- 34 H. R. Shaterian, A. Hosseinian and M. Ghashang, *Tetrahedron Lett.*, 2008, **49**, 5804.
- 35 M. Dabiri, A. S. Delbari and A. Bazgir, *Heterocycles*, 2007, **71**, 543.
- 36 S. B. Patil, P. R. Singh, M. P. Surpur and S. D. Samant, *Ultrason. Sonochem.*, 2007, **14**, 515.
- 37 A. Zare, A. Hasaninejad, A. Salimi Beni, A. R. Moosavi-Zare, M. Merajoddin, E. Kamali, M. Akbari-Seddigh and Z. Parsaee, *Sci. Iran., Trans. C*, 2011, **18**, 433.
- 38 A. K. Gupta, A. S. Curtis and J. Mater, *J. Mater. Sci.: Mater. Med.*, 2004, **15**, 493.
- 39 T. Neuberger, B. Schoepf, H. Hofmann, M. Hofmann and B. von Rechenberg, *J. Magn. Magn. Mater.*, 2005, **293**, 483.
- 40 Q. A. Pankhurst, J. Connolly, S. K. Jones and J. Dobson, *J. Phys. D: Appl. Phys.*, 2003, **36**, 167.
- 41 D. Wang, J. He, N. Rosenzweig and Z. Rosenzweig, *Nano Lett.*, 2004, **4**, 409.
- 42 C. Xu, K. Xu, H. Gu, R. Zheng, H. Liu, X. Zhang, Z. Guo and B. Xu, *J. Am. Chem. Soc.*, 2004, **126**, 9938.
- 43 J. M. Perez, F. J. Simeone, Y. Saeki, L. Josephson and R. Weissleder, *J. Am. Chem. Soc.*, 2003, **125**, 10192.
- 44 D. L. Graham, H. A. Ferreira and P. P. Freitas, *Trends Biotechnol.*, 2004, **22**, 455.
- 45 R. Hiergeist, W. Andra, N. Buske, R. Hergt, I. Hilger, U. Richter and W. Kaiser, *J. Magn. Magn. Mater.*, 1999, **201**, 420.
- 46 A. Jordan, R. Scholz, P. Wust, H. Fahling and R. Felix, *J. Magn. Magn. Mater.*, 1999, **201**, 413.
- 47 M. Shokouhimehr, Y. Piao, J. Kim, Y. Jang and T. Hyeon, *Angew. Chem., Int. Ed.*, 2007, **46**, 7039.
- 48 R. Tayebee, M. M. Amini, N. Abdollahi, A. Aliakbari, S. Rabiee and H. Ramshini, *Appl. Catal., A*, 2013, **468**, 75.
- 49 L. Wang, J. H. Han, T. Sheng, J. Z. Fan and X. Tang, *Synlett*, 2005, 337.
- 50 N. Azizi, L. Torkian and M. R. Saidi, *J. Mol. Catal. A: Chem.*, 2007, **275**, 109.
- 51 S. Sobhani, E. Safaei, A. R. Hasaninejad and S. Rezazadeh, *J. Organomet. Chem.*, 2009, **694**, 3027.
- 52 R. Tayebee, F. Nehzata, E. Rezaei-Sereshta, F. Z. Mohammadi and E. Rafiee, *J. Mol. Catal. A: Chem.*, 2011, **351**, 154–164.
- 53 G. P. Romanellia, D. M. Ruiza, H. P. Bideberripea, J. C. Autinob, G. T. Baronetti and H. J. Thomasa, *ARKIVOC*, 2007, **16**, 1.
- 54 G. Baronetti, L. Briand, U. Sedran and H. Thomas, *Appl. Catal., A*, 1998, **173**, 265.
- 55 D. Lyon, W. Miller, T. Novet, P. Domaille, E. Evitt, D. Johnson and R. Finke, *J. Am. Chem. Soc.*, 1991, **113**, 7209.
- 56 (a) X. Liu, Z. Ma, J. Xing and H. Liu, *J. Magn. Magn. Mater.*, 2004, **270**, 1; (b) A. Tarlani, M. Abedini, M. Khabaz and M. M. Amini, *J. Colloid Interface Sci.*, 2005, **292**, 486.
- 57 B. Helms, S. J. Guillaudeu, Y. Xie, M. McMurdo, C. J. Hawker and J. M. J. Frechet, *Angew. Chem., Int. Ed.*, 2005, **44**, 6384.
- 58 X. F. Yu, Y. C. Zou, S. J. Wu, H. Liu, J. Q. Guan and Q. B. Kan, *Mater. Res. Bull.*, 2011, **46**, 951.
- 59 B. Voit, *Angew. Chem., Int. Ed.*, 2006, **46**, 4238.
- 60 J. D. Bass and A. Katz, *Chem. Mater.*, 2006, **18**, 1611.
- 61 D. Coutinho, S. Madhugiri and K. J. Balkus, *J. Porous Mater.*, 2004, **11**, 239.
- 62 J. Alauzun, A. Mehdi, C. Reyé and R. J. P. Corriu, *J. Am. Chem. Soc.*, 2006, **128**, 8718.
- 63 A. P. Wight and M. E. Davis, *Chem. Rev.*, 2002, **102**, 3589.
- 64 N. E. Leadbeater and M. Marco, *Chem. Rev.*, 2002, **102**, 3217.
- 65 R. K. Zeidan, S. J. Hwang and M. E. Davis, *Angew. Chem., Int. Ed.*, 2006, **45**, 6332.
- 66 D. Astruc, F. Lu and J. R. Aranzas, *Angew. Chem., Int. Ed.*, 2005, **44**, 7852.
- 67 K. Motokura, N. Fujita, K. Mori, T. Mizugaki, K. Ebitani and K. Kaneda, *J. Am. Chem. Soc.*, 2005, **127**, 9674.
- 68 R. K. Zeidan and M. E. Davis, *J. Catal.*, 2007, **247**, 379.
- 69 F. Gelman, J. Blum and D. Avnir, *Angew. Chem., Int. Ed.*, 2001, **40**, 3647.
- 70 T. Q. Zeng, W.-W. Chen, C. M. Cirtiu, A. Moores, G. Song and C.-J. Li, *Green Chem.*, 2010, **12**, 570.
- 71 R. Tayebee, M. M. Amini, F. Nehzat, O. Sadeghi and M. Armaghan, *J. Mol. Catal. A: Chem.*, 2013, **366**, 140.
- 72 R. Tayebee, M. M. Amini, M. Ghadamgahi and M. Armaghan, *J. Mol. Catal. A: Chem.*, 2013, **366**, 266.
- 73 G. Jian, C. Yaguang, Q. Lunyuand and L. Qin, *Polyhedron*, 1996, **15**(13), 2273.
- 74 Y. Liu, P. Liu, Z. Su, F. Li and F. Wen, *Appl. Surf. Sci.*, 2008, **255**, 2020.
- 75 G. Baronettia, L. Brianda, U. Sedranb and H. Thomasa, *Appl. Catal., A*, 1998, **172**, 256.
- 76 Y. Li, H. Chen, C. Shi, D. Shi and S. Ji, *J. Comb. Chem.*, 2010, **12**, 231.
- 77 B. Das, K. Laxminarayana, B. Ravikanth and B. R. Rao, *J. Mol. Catal. A: Chem.*, 2007, **26**, 180.
- 78 H. R. Shaterian, H. Yarahmadi and M. Ghashang, *Bioorg. Med. Chem. Lett.*, 2008, **18**, 788.
- 79 W. Q. L. Jiang, T. J. An and P. Zou, *Chin. J. Chem.*, 2008, **26**, 697.
- 80 R. A. Marcus, *Annu. Rev. Phys. Chem.*, 1964, **15**, 155.
- 81 M. M. Khodaei, A. R. Khosropour and H. Moghanian, *Synlett*, 2006, 916.
- 82 S. B. Patil, P. R. Singh, M. P. Surpur and S. D. Samant, *Synth. Commun.*, 2007, **37**, 1659.

- 83 G. C. Nandi, S. Samai, R. Kumar and M. S. Singh, *Tetrahedron Lett.*, 2009, **50**, 7220.
- 84 J. Wen-Qing, A. Li-Taoa and Z. Jian-Ping, *Chin. J. Chem.*, 2008, **26**, 1697.
- 85 M. R. M. Shafiee, R. Moloudi, N. T. Jervekani and M. Ghashang, *Adv. Mater. Res.*, 2012, **535**, 851.
- 86 A. Zare, A. R. Hasaninejad, E. Rostami, A. R. Moosavi-zare, N. Pishahang, M. Roshankar, F. Khedri and M. Khedri, *Elec. J. Chem.*, 2010, **7**(4), 1162.
- 87 K. S. Niralwad, B. B. Shingate and M. S. Shingare, *Chin. Chem. Lett.*, 2011, **22**, 551.